Journal of *Marine Science and Engineering*

MDPI

Article

Microbubbles as Proxies for Oil Spill Delineation in Field Tests

Yaomei Wang [1,*], Worakanok Thanyamanta [1], Craig Bulger [2], Neil Bose [1] and Jimin Hwang [3]

[1] Department of Ocean and Naval Architectural Engineering, Memorial University of Newfoundland, St. John's, NL A1B 3X7, Canada; s02wt@mun.ca (W.T.); nbose@mun.ca (N.B.)
[2] Centre for Applied Ocean Technology, Fisheries and Marine Institute of Memorial University of Newfoundland, St. John's, NL A1C 5R3, Canada; Craig.Bulger@mi.mun.ca
[3] Australian Maritime College, University of Tasmania, Launceston, TAS 7250, Australia; jimin.hwang@utas.edu.au
* Correspondence: yaomeiw@mun.ca

Abstract: To overcome the environmental impacts of releasing oil into the ocean for testing acoustic methods in field experiments using autonomous underwater vehicles (AUVs), environmentally friendly gas bubble plumes with low rise velocities are proposed in this research to be used as proxies for oil. An experiment was conducted to test the performance of a centrifugal-type microbubble generator in generating microbubble plumes and their practicability to be used in field experiments. Sizes of bubbles were measured with a Laser In-Situ Scattering and Transmissometry sensor. Residence time of bubble plumes was estimated by using a Ping360 sonar. Results from the experiment showed that a larger number of small bubbles were found in deeper water as larger bubbles rose quickly to the surface without staying in the water column. The residence time of the generated bubble plumes at the depth of 0.5 m was estimated to be over 5 min. The microbubble generator is planned to be applied in future field experiments, as it is effective in producing relatively long-endurance plumes that can be used as potential proxies for oil plumes in field trials of AUVs for delineating oil spills.

Keywords: microbubbles; proxy; oil spill; sonar; size of bubbles; residence time

Citation: Wang, Y.; Thanyamanta, W.; Bulger, C.; Bose, N.; Hwang, J. Microbubbles as Proxies for Oil Spill Delineation in Field Tests. *J. Mar. Sci. Eng.* **2021**, *9*, 126. https://doi.org/10.3390/jmse9020126

Academic Editor: Mario Brito
Received: 18 December 2020
Accepted: 22 January 2021
Published: 27 January 2021

1. Introduction

An accidental oil spill can be a major threat to public health resulting in a variety of environmental impacts as well as fatal consequences to the marine ecosystem [1]. Rapid response and the use of appropriate detection methods and sensors are key to mitigate the undesirable consequences of a spill accident. When released, oil is broken up by turbulence into droplets of various sizes where large droplets tend to rise rapidly to the surface while small droplets tend to be transported horizontally by ocean currents [2]. Small oil droplets released in the subsurface, particularly those treated with chemical dispersant can stay in the water column for hundreds of hours and form subsurface plumes [3,4]. Detecting these subsurface plumes attracts our interest as it is an ideal task for AUVs that collect and communicate high resolution information of the plumes in near real-time from the subsurface, a task unachievable by many traditional methods including remote sensing.

The clustering of oil plumes in general ocean conditions is a distinct characteristic that poses challenges in detecting oil plumes with submersible sensors that have been commonly used in the field including fluorometers, particle size analyzers and other chemical sensors [5]. By using these sensors and conventional point-based in-situ measurements onboard an autonomous underwater vehicle (AUV), gradient methods have been widely employed to track an oil plume [6]. However, recent experiments done by our research team have revealed severe limitations of in-situ sensors as a primary sensor to conduct an adaptive mission [7,8], which allows the path of the AUV to be updated and optimized based on real-time sensor data. The clustering characteristics of oil in water can inherently generate consecutive noise-like positive and negative peaks from a fluorometer that might confuse an autonomous signal processor algorithm. The system would have

to determine whether these peaks are true positive signals or noise from other possible unknown sources. Hence, gradient approaches using single point sensors are likely to cause confusion to maneuver an AUV in real-time [7]. In addition, a point-based sensor can only take measurements where the vehicle is located. As a result, the vehicle must be constantly moving in order to carry out continuous measurements and cannot pre-detect the target oil without entering inside of the body of a plume. It also implies that the survey design requires a relatively high resolution, hence an exhaustive search by the vehicle, to acquire reasonably comprehensive information of the plume such as oil concentrations and its approximate extent. This is neither efficient nor suitable to conduct an adaptive mission. Another common sensor used to detect oil droplets in water is an optical laser diffraction instrument which measures the sizes of particles suspended in water based on scattering technology. The data provided by this sensor may lead to ambiguity especially in the non-confined real ocean that may contain a great number of natural particles. Without measuring additional morphological information of the detected particles in real-time, it is not feasible to differentiate the regular shapes that oil droplets would have from those of other substances in nature.

To overcome these challenges, acoustic backscattering has been used as an alternative means to detect oil plume [9]. Acoustic devices such as sonars utilize remote detection approach to capture and visually display acoustic backscatters of dynamically dispersing oceanographic targets including oil droplets and methane bubbles in the water column. As such, using this method allows for the use of buoyant acoustic backscattering materials as tracers in field studies.

Another challenge in oil spill research is the ability to perform field experiments in oil spill conditions, as it is inappropriate to release oil into the ocean. Dye tracers, such as Rhodamine WT, are typically used to study oceanographic processes including dispersion of spilled oil as they can be detected effectively at low concentrations [10]. However, as these tracers are water-soluble, they do not behave like oil which can be distributed in the water column as dispersed, dissolved, and gas phases [11,12].

Gas bubbles have a potential of being used as proxies for oil as they are expected to reasonably represent the patchy characteristics oil plumes once released into the ocean. Gas bubbles are environmentally friendly and can be detected well by sonar sensors. Similar to oil droplets, they are buoyant and do not dissolve readily in the water column and thus they are expected to show similar clustering characteristics of oil in water. In addition to their similar transport behaviors in ocean waves and currents, oil droplets and gas bubbles are both acoustic scatters and can be detected by sonars. When released continually, they can form bubble clouds or plumes similar to plumes of oil spills, which can be used during AUV field trials. As gas bubbles rise more quickly than oil droplets, bubbles of micron size, also known as microbubbles, are proposed here for being used as the oil proxy. Definition of microbubbles in the field of fluid physics are bubbles of diameters less than 100 μm [13]. Different from typical bubbles which rise to the surface and burst, microbubbles rise up and shrink before disappearing in the liquid [14]. These tiny bubbles have low buoyancy and slow rise velocities allowing them to stay in the water column for some period until they are detected by sonars equipped on AUVs. Microbubbles have been widely studied and used in various fields including water treatment, water purification, mineral processing, natural ecology restoration, cleaning and medicine [13,15]. Different types of microbubble generators have been developed for large scale applications and many are commercially available.

In this paper, we propose the use of gas bubble as a proxy for oil in AUV field missions. This paper presents an initial investigation on the suitability of using air bubbles as proxies for oil droplets. We did not aim to replicate oil droplets but to find some kind of tracer that generates plumes that could be detected by acoustic devices in AUVs. For this purpose, our main interest was the residence time and distribution of gas bubble plumes in the water column to demonstrate that bubble plumes could represent the buoyant characteristics of oil plumes and could stay in the water for a period of time before being detected by

acoustic devices. As acoustic backscatters of oil and gas are different, it is not necessary for the bubble plume to have the same quantities of bubbles as oil droplets in order to be effectively detected by acoustic sensors. To prove this concept, we evaluated plumes of air bubbles generated by a commercial microbubble generator and used a sonar sensor to detect the generated plumes. Results from the experiment and the suitability of using microbubbles for oil spill detection studies are presented and discussed.

2. Sonar Applications for Oil and Gas Detection

2.1. Previous Work

Sonar systems have been used to measure the sizes of oil droplets [16], to detect the oil under surface ice, encapsulated in ice, and sunken on the seafloor [17–20], to measure concentrations of oil and gas in the water column [21,22], and to measure the flow rates of oil released during a spill event [23].

Sonars have an advantage over point-based in-situ sensors when used to detect subsurface oil as they can cover a large continuous area as opposed to sampling a discrete volume of the water column [24]. Fluorometers, the most commonly used point-based in-situ oil sensors, are also susceptible to false positives due to disturbance from natural sources of fluorescence present in seawater [25]. In order to attain effective detection of oil in the water column, a combination of multiple methods employing different working principles are typically required. The use of sonars in conjunction with fluorometers can increase reliability of the detection and help confirm the existence of the oil [26]. Sonars detect oil by recording the backscattered sound from oil droplets [27]. The strength of the backscattering is determined by the acoustic impedance contrast between the oil and ambient water [28]. The advantages of sonar systems include the capability of seeing a long distance, seeing at low visibility, and provide quantitative information from acoustic backscatter when the frequency of the system is sufficiently high [17]. Besides, sonar systems are less affected by the bio-fouling compared to the Laser In-Situ Scattering and Transmissometer (LISST) when measuring the size of oil droplets [16].

Sonars are capable of distinguishing two fluids with low impedance contrast, such as crude oil and seawater, and detecting oil at low concentrations [28]. This was proven in a study where a 400 kHz Wide Band Multi-Beam sonar was used to effectively detect freshwater injected into the saltwater, two fluids with small difference in reflectivity [29]. Another test performed at the Navy facility Oil and Hazardous Materials Simulated Environmental Test Tank, New Jersey of the U.S. showed that sonars with a nominal operating frequency of 400 kHz were able to capture a well-dispersed plume with low oil-in-water concentrations [9]. The result exceeded the expectation of a high-frequency sonar to detect oil at low concentration. For detection of gas bubbles, such as greenhouse gas methane, sonar is the most commonly used sensor as gas bubbles have strong acoustic scattering [30–32]. In the work of Uchimoto et al. [33], the experiment found that a 600 kHz side-scan sonar could detect underwater CO2 bubbles of 1–2 mm and 1 cm in diameter, the sizes of natural seep bubbles [34]. Moreover, sonars are superior to underwater video cameras in surveying well-dispersed gas bubbles as videos are restricted to smaller areas [32,35].

As there were no industry-accepted means to measure the flow rate of the hydrocarbon fluid, an acoustic imaging sonar (1.8 MHz) and an acoustic Doppler sonar (1.3 MHz) were used to measure the flow rates of the hydrocarbon released from the Deepwater Horizon Macondo well on 31 May 2010 [23]. The acoustic imaging sonar was used to record horizontal cross-section images of the flowing fluid, while the Doppler sonar provided vertical velocities of the flow. The method used provided consistent result with other studies such as in [36], which verified usefulness of sonar systems and suitability of sonars for oil detection.

The effectiveness sonars in detecting oil droplets and gas bubbles is highly dependent on their operating frequencies. Weber et al. used an acoustic method to quantify the amount of oil surfacing with ship-mounted acoustic Simrad ES60 echo sounders [37]. These echo sounders were operated at the frequencies of 12, 38 and 200 kHz. The anomalously high

return detected by the 200-kHz echo sounder above the depth of 200 was in accordance with the visual observation of the oil from the surface. However, similar anomalous backscattering was not observed by the echo sounders operating at lower frequencies of 12 and 38 kHz. Another study used a sonar with the operating frequency of 5 MHz to measure oil droplets size in an oil-water-dispersant mixture [16]. The frequency of the sonar was much higher than the resonant frequency for the size of detected oil droplets. The comparison with measurements from a LISST sensor showed a good performance of the acoustic method. From the above studies, high operating frequencies tend to provide better oil detection. However, the frequency should not be too high as the signal attenuation will increase at a higher frequency leading to a shorter range of the sonar [16]. The optimum frequency of a sonar depends on the size of oil droplets, the coverage distance, and the level of ambient noise [27]. A tank experiment with the use of an Acoustic Zooplankton and Fish Profiler multiple-frequency echo sounder showed that the submerged oil was detectable with the frequencies of 455, 769, 1250 and 2000 kHz [38]. Results from the study showed that the size of oil droplets was in the order of 100 µm [38]. Moreover, the lower frequency could be also effective in detecting oil droplets if the size of the droplets was larger. Similarly, the size of gas bubbles is essential when selecting the frequency of a sonar. Szczucka [39] noted that "acoustic determination of the concentration of gas bubbles in the sea is based on the phenomenon of resonant backscattering" and "a bubble of a definite size resonates with an incident acoustic wave of a precisely defined frequency, inversely proportional to a bubble radius".

Types of sonars are also important in selecting a sonar system for oil and gas detection. The types of sonars that have been used to detect suspended oil droplets and gas bubbles include echo sounders, sider-scanning sonars, multibeam sonars [35,40–42]. Multibeam echo sounders excelled the single-beam echo sounders in determining the plume's geometric feature [32]. An experiment with a focus on detecting sunken oil on the sea bottom compared capabilities of various types of sonars including a side-scan sonar, a multibeam/panoramic sonar, a 3D acoustic camera, and a front-looking sonar, with frequencies ranging from 100 kHz to 600 kHz. The high-frequency sonars (200–500 kHz) were found to have the ability to detect oil patches with low reflectivity. The side-scan sonar can quickly find the position of oil as a wide swath. More precise detection was achieved from the multibeam sonar, the 3D acoustic camera, and the front-looking sonar [20]. These findings related to sunken oil can be used as a reference when considering the application of sonars in detecting oil droplets and gas bubbles in the water column.

To confirm the potential use of sonar for oil detection in future AUV experiments, proof-of-concept experiments were conducted as described below.

2.2. Proof-of-Concept Sonar Experiment

Aiming to overcome the challenges in using point-based in-situ sensors in AUV oil spill missions, we investigated the use of sonar in future AUV experiments. Two sonar instruments were tested for proof-of-concept. A set of tests were conducted in the wave tank facility at the Bedford Institute of Oceanography (BIO), Dartmouth, Nova Scotia, Canada on 31 July 2019 [43]. The facility is operated by the Centre for Offshore Oil, Gas and Energy Research (COOGER), Department of Fisheries and Oceans Canada. Alaska North Slope (ANS) crude oil and two different sonar sensors were selected for the test: the BV5000 3D scanning sonar and the M450 2D sonar of Teledyne Blueview. The frequencies of these sonars were 1.35 MHz and 450 kHz, respectively. The results demonstrated that both sonars were capable of detecting oil in advance of an AUV (by using a forward-looking sonar) and at a distance, unlike other in-situ oil sensors that had been used to date. An oil plume consisting of a number of small droplets as well as a significant amount of noise were detected by the M450 sonar. By comparison, the acoustic pings at higher frequency generated by the BV5000 resulted in clearer sonar images at a distance of 2.5 m from the sonar head. The fan-shaped sonar images also captured the upward moving process of the plume as it rose to the surface. These proof-of-concept-test results indicated that acoustic

sensors may have the following potential advantages in detecting oil from an AUV in the ocean:

1. An oil plume can potentially be pre-detected by an AUV prior to entering the plume.
2. Sonar fan-shaped image display is more suitable than point-based oil sensors for discontinuous oil patches to make an adaptive decision on the next waypoints or trajectory to delineate the plume.
3. The two-dimensional survey of the scanning sonar has advantages over a point-based survey to undertake an adaptive mission for a dynamically dispersing target such as an oil plume.

3. Experiment Setup

In this study, we propose using gas bubbles as environmentally friendly proxy for oil in AUV field experiments so as to allow AUVs equipped with sonars to be tested in realistic oil spill conditions without releasing oil into the ocean. When bubbles are generated with hydrocarbon gas, such as methane or butane, a sonar can be used with hydrocarbon gas sensor for cross-validation. However, in our experiments, air bubbles were used to minimize health and environmental risks posed by releasing hydrocarbon gases, such as methane which is a known greenhouse gas. The proposed gas bubble plumes were generated using a commercial microbubble generator. Microbubbles have slow rise velocity leading to plumes that remain in the water column for a period of time before being detected by a sonar and/or other sensors. An experiment was conducted to test the microbubble generator in creating bubble plumes and characterize the plumes in terms of bubble size, residence time, and suitability to be used in the ocean. The experiment also aimed to evaluate a sonar sensor on its performance in detecting the bubble plumes.

3.1. Bubble Gennerator

The system that we tested was a microbubble pump, Karyu Turbo Mixer (KTM) pump, developed by Nikuni Co., Ltd. in Kawasaki, Kanagawa, Japan, (see Figure 1). The centrifugal pump uses a principle similar to the dissolved air flotation method [44]. However, the air dissolution and mixing occur simultaneously as the air and water are drawn in and pressurized by the mechanics of the uniquely designed turbine impeller. A combination of frictional, axial, and centrifugal forces created by the impeller helps enhance entrainment of air by breaking the air into small bubbles and generating high operating pressure [45]. Atmospheric air is drawn into the low-pressure suction side of the pump eliminating the need of an air compressor. A large mixing tank is also not required leading to a more compact system that is suitable to be used at sea if needed. The average size of the microbubbles produced by this system is 25 µm but a dimeter of less than 10 µm can be obtained by varying operating conditions including air and water flowrates and pressure [46].

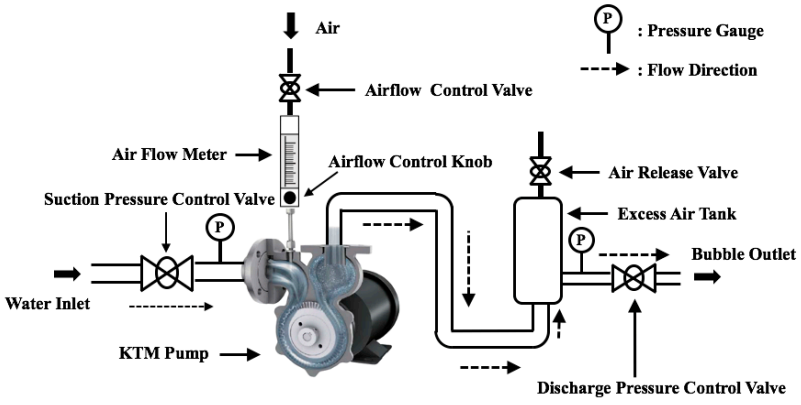

Figure 1. A sketch of the microbubble generator with the use of KTM pump.

3.2. Sensor Suite

The sonar used in the experiment was a Ping360 sonar from Blue robotics, Torrance, CA, USA (see Figure 2). Specifications of the sonar are presented in Table 1. The Ping360 is a mechanical scanning imaging sonar (see Figure 2) that has a 50 m range and can work to a depth of 300 m. It was designed to be used for navigation on ROVs such as BlueROV2 [47], but can also be used for obstacle avoidance, inspection, tracking, and so on. In the experiment, we used the Ping360 to detect microbubbles generated by the KTM pump and evaluated the residence time of bubbles. In this paper, the residence time was the length of time that the bubble plume stayed in the water column at one depth (within the vertical range of the sonar) as captured by the sonar.

Figure 2. Ping360 mechanical scanning imaging sonar.

The sizes of bubbles generated by the microbubble generator were measured using a Laser in-situ Scattering and Transmissometry (LISST-200X) sensor (see Figure 3) LISST-200X, developed by Sequoia Scientific Inc. in Bellevue, WA, USA, was designed for measuring particle sizes and concentrations in water. The LISST-200X is rated to a depth of 600 m and can cover a size range between 1 and 500 microns, which is the range of our interest [48]. Other measurements provided by LISST-200X also include temperature and depth.

Figure 3. LISST-200X.

Table 1. Specifications of Ping360 [49].

Parameter	Value
Frequency	750 kHz
Supply Voltage	11–25 volts
Beamwidth (Horizontal)	2°
Beamwidth (Vertical)	25°
Working Range	0.75–50 m
Weight in Air	510 g
Scan Speed at 2 m	9 s/360°
Scan Speed at 50 m	35 s/360°
Range Resolution	0.08% of the range

4. Experiment and Results

4.1. Experimental Setup

A detailed experiment was conducted in the tow tank of the Ocean Engineering Research Centre (OERC) at the Memorial University of Newfoundland (see Figure 4). The tank has a length of 54 m which was beneficial as the dispersion of the microbubbles was not restricted by the tank boundaries. The observation window looking into the side of the tow tank helped to capture the motion of the bubbles. The tank was filled with clean water before the experiment which was favorable for the measurements of the sonar and the LISST-200X. Figure 5 shows the setup of the KTM microbubble generator on a bridge in the tow tank.

Figure 4. OERC tow tank of Memorial University of Newfoundland.

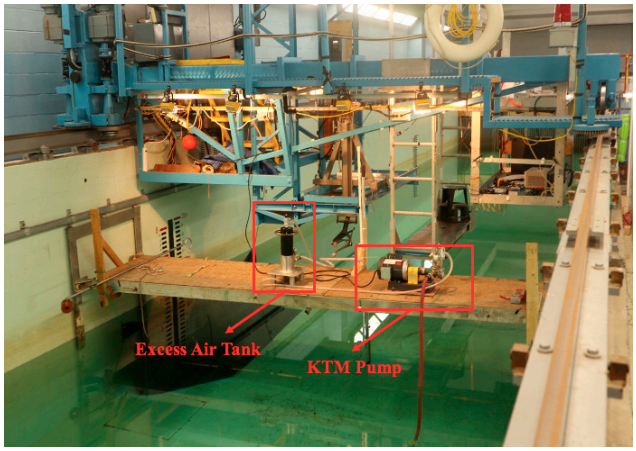

Figure 5. The setup of the Nikuni KTM pump in the tow tank.

In the experiment, the LISST-200X sensor was set up in front of the release nozzle; the bubble cloud passed through the sensing range of the LISST-200X (see Figure 6). The Ping360 sonar was placed to one side of the release nozzle, with its horizontal scanning direction covering the passing plume. Nine sets of sampling positions were selected to precisely measure the distribution and motion of the bubbles (see Table 2 and Figure 7). The horizontal and vertical distances between adjacent sampling positions were selected to be 0.5 m to cover the length and height of the plume based on visual observation. In our experiment, the water in the tank remained static except for the disturbance from the water and bubbles coming from the discharge nozzle.

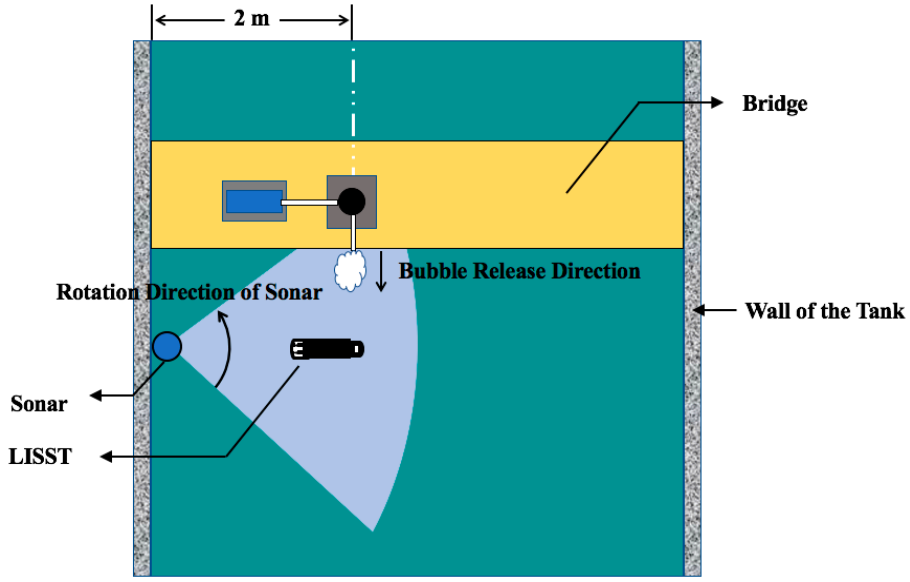

Figure 6. Top view of the setup of the sonar and LISST-200X in the tow tank.

Table 2. The number of test and corresponding positions of sonar and LISST-200X.

Test No.	Position of Sonar	Position of LISST-200X
1	1	A
2	2	B
3	3	C
4	4	D
5	5	E
6	6	F
7	7	G
8	8	H
9	9	I

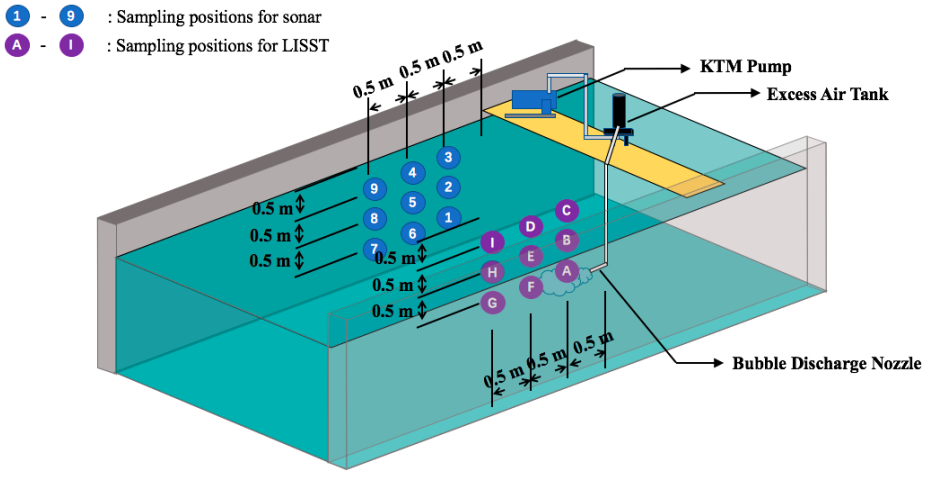

Figure 7. Sampling positions for the sonar and LISST-200X in the tow tank.

The sequence of the tests is indicated by the red arrows shown in Figure 8. When the sonar and the LISST were set in their positions, these two sensors were started up to collect background information for one minute. This background information was a reference for calculating the residence time of bubbles. Then, the bubble generator was turned on to generate bubbles for more than 3 min in order to get stable a plume. The bubble generator

was then stopped and the sonar and the LISST continued their measurements until there was no clear plume visible in the sonar image. The amount of time after pump was shut off until the plume disappeared from the sonar image was approximated as the residence time of the bubbles in the water at the specified depth. The bubble plume generated by the KTM pump can be seen in Figure 9.

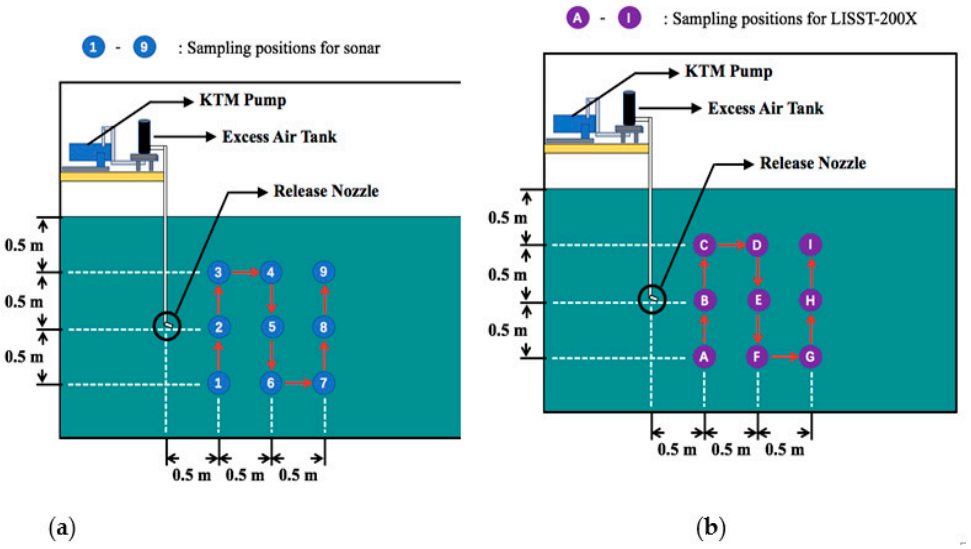

Figure 8. Side view of the sampling positions for (**a**) sonar and (**b**) LISST-200X in the tow tank.

Figure 9. Bubble plume generated by the KTM pump in the tow tank.

4.2. Measurements from the Experiment

4.2.1. Bubble Size Distribution

The size distributions of the bubbles collected by the LISST-200X sensor at the 9 sampling positions when the bubble generator was working are shown in Figure 10. This can help understand size distribution of the bubbles at different locations within the plume. The sampling position C, D, and I were at a higher altitude than the release nozzle, the sampling position B, E, and H were at the same depth as the release nozzle, and the sampling position A, F, and G were lower than the release nozzle. From the bubble size distribution, it can be observed that:

1. A higher proportion of smaller bubbles was found at deeper positions. For example, at position F which was at a depth of 1.5 m, more than 90% of the bubbles were smaller than 100 microns, while at position E which was at the depth of 1.0 m, the

majority were within the range of 100–150 microns. At a shallower position (position D), more large bubbles between 200 and 250 microns were found. The difference in size distribution at varied depths was owing to the rise velocities of differently sized bubbles. Large bubbles rose quickly toward the water surface while small bubbles rose more slowly leading to a larger proportion of small bubbles staying at depth.

2. A larger percentage of smaller bubbles were collected at the farthest distance from the release nozzle. For example, at the water depth of 1.5 m, only 80% of bubbles found at position A were smaller than 100 microns while almost all the bubble (99%) found at position G were smaller than 100 microns. For position C, D, and I, a larger proportion of bubbles with sizes smaller than 250 microns were collected at position I, the longest distance from the release nozzle among the 3 positions placed at 0.5 m water depth.

The variation of bubble sizes in the horizontal direction was partly impacted by the different rise velocities of the bubbles where larger bubbles, having higher rise speeds velocities, surfaced quickly without travelling a long distance horizontally. In addition, in the experiment, the release nozzle released the bubbles at an angle of inclination of 20° (see Figure 11), which defined the path of the plume and made bubbles, especially smaller bubbles as they tend to travel horizontally rather than upwards, go to deeper water as they moved further away from the nozzle.

There was also some exception to the size distribution in the horizontal direction. For example, at the water depth of 1.0 m, bubbles smaller than 150 microns comprised more than 50% of the bubbles found at position H, and only 41% for position E. However, at position B which was closest to the release nozzle, a higher percentage of more than 70% were observed. At both C and I, 3% of bubbles were between 50–100 microns while there were no bubbles in this size range at position D. 37% of bubbles at position C was in the size range of 100–200 microns, 32% of bubbles at position D were in the size range of 100–200 microns, and 32% of bubbles at the position I were in the size range of 100–200 microns.

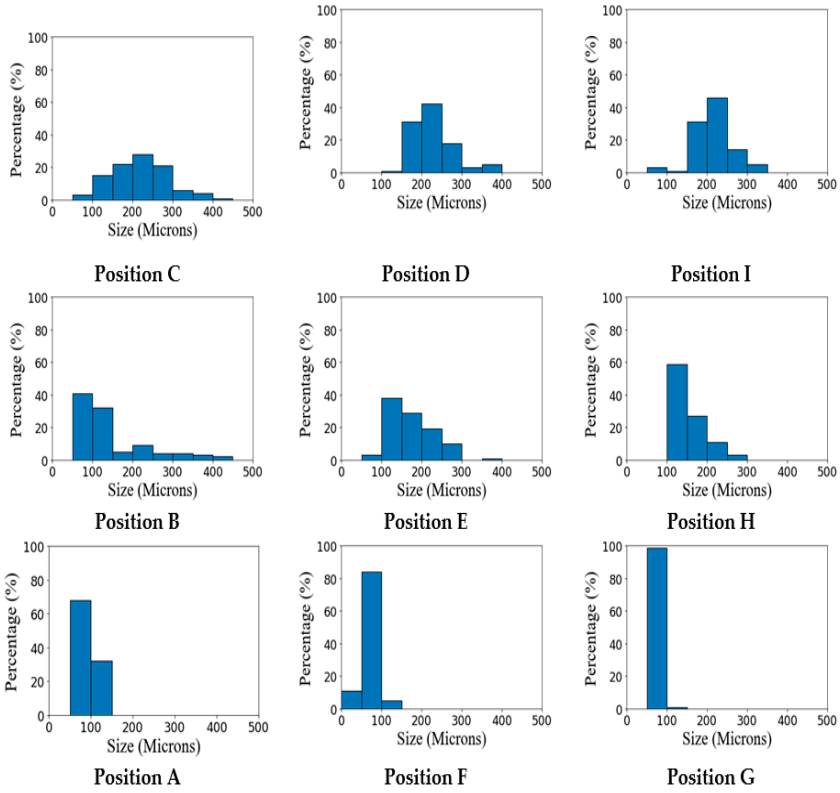

Figure 10. Distribution of the bubble size at 9 sampling positions.

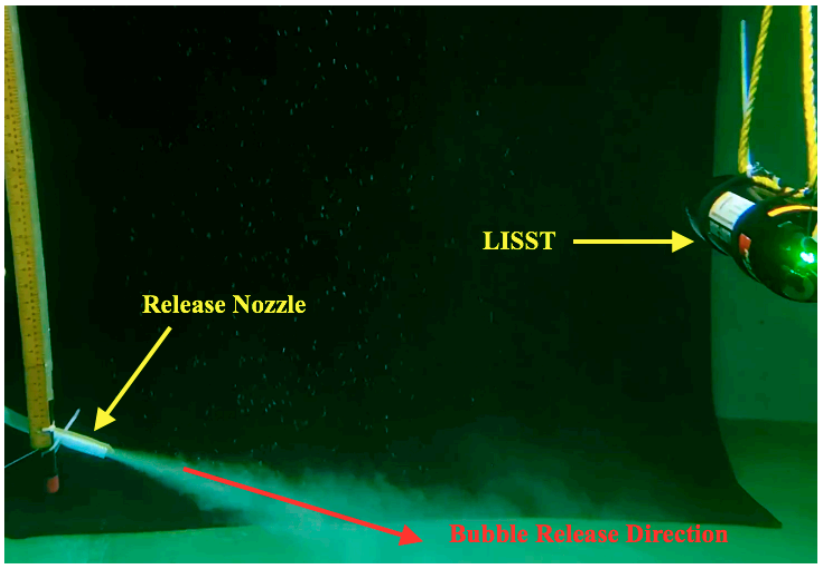

Figure 11. Bubbles released from the nozzle.

4.2.2. Residence Time of Bubbles

The residence time of bubbles was estimated based on sonar images. The length of time from when the bubble generator was stopped until the time when no clear bubble plume could be observed from the sonar image was assumed to be the residence time of bubbles in the water column. In this experiment, it was assumed that the highest concentration of bubbles was on the vertical plane along the centerline of the plume and parallel to the side wall of the tank (Plane A in Figure 12). Therefore, the length of time that bubbles stayed on this plane after the bubble generator was shut off was measured as the residence time. As the sonar used was a mechanical scanning sonar and had a vertical beamwidth of 25°, the residence time of bubbles measured at sampling point 1 represents the residence time of the bubbles within the rectangle area (region 1) in Figure 13, which overlaps the sampling region of point 2.

The sonar images collected from position 3 before the start of the bubble generator, when the bubble generator was working, and when there was no plume on the vertical plane for calculating residence time are presented in Figure 14. In Figure 14c, there were no visible bubbles in the sonar image in region 1 and above, which was regarded as the disappearance of bubbles.

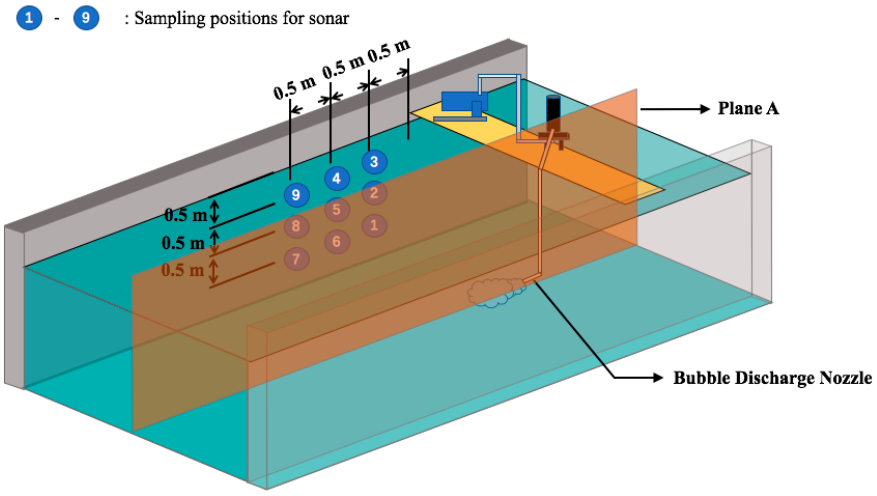

Figure 12. Sketch of plane A that intersected the release nozzle and was parallel to the sidewall of the tank which was used for measuring the residence time of bubbles.

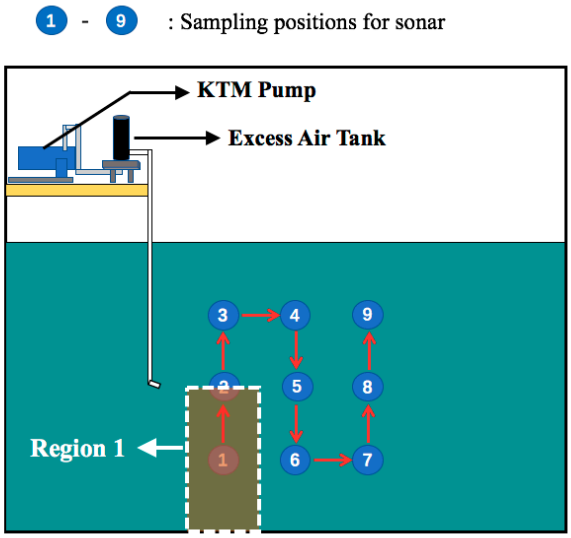

Figure 13. Sketch of the area that was used to measure the residence time of bubbles detected by the sonar at sampling point 1.

The residence times of bubbles calculated at the nine sampling positions are presented in Table 3.

Table 3. Residence time of bubbles calculated at different sampling positions from sonar.

	Distance *: 0.5 m	Distance: 1.0 m	Distance: 1.5 m
Depth: 0.5 m	Position 3:	Position 4:	Position 9:
	304 s	364 s	323 s
Depth: 1.0 m	Position 2:	Position 5:	Position 8:
	106 s	148 s	214 s
Depth: 1.5 m	Position 1:	Position 6:	Position 7:
	65 s	77 s	133 s

* Distance means the horizontal distance from sonar to the nozzle which is shown in Figure 7.

1. The residence time decreased with an increase in water depth. One can expect bubbles to rise up from deeper to shallower water. Therefore, the residence time measured at a shallower position, e.g., position 3, can be considered to be the length of time from the first bubbles appeared in this shallow water region when the bubble generator was stopped until the time when the last bubble that rose from the deeper water to this region disappeared.
2. In most cases, the residence time of bubbles increased with the distance from the release nozzle. This was because the release nozzle had an inclination angle which drove the bubbles deeper away from the nozzle. There was an exception at the depth of 0.5 m where the residence times of bubbles at position 3, 4, and 9 were 304 s, 364 s, and 323 s respectively. For position 9, the residence time of the bubbles was shorter than that collected at position 4. Considering position 9 to be the furthest point from the center of the plume, this phenomenon was possibly caused by bubbles disappearing due to shrinking or dissolution of the gas as they rose through the water column toward the surface. Besides, at a longer distance from the nozzle, the low density of bubbles at shallower depth also affected the images collected by the sonar, which affects the calculation of residence time at the end. Moreover, the residence times obtained at these positions may have been affected by the bubbles that rose up from positions directly underneath them (position A, F, and G, respectively). As position F had a higher percentage of bubbles below the size of 50 microns compared

with position A and G, these bubbles may have risen up slowly to the depth of 0.5 m, contributing to longer residence time collected at position 4. This was also witnessed at position A and G. Position G has a higher percentage of small bubbles within the size range of 50–100 microns than position A, which probably resulted in the residence time collected at position 9 being longer than that at position 3.

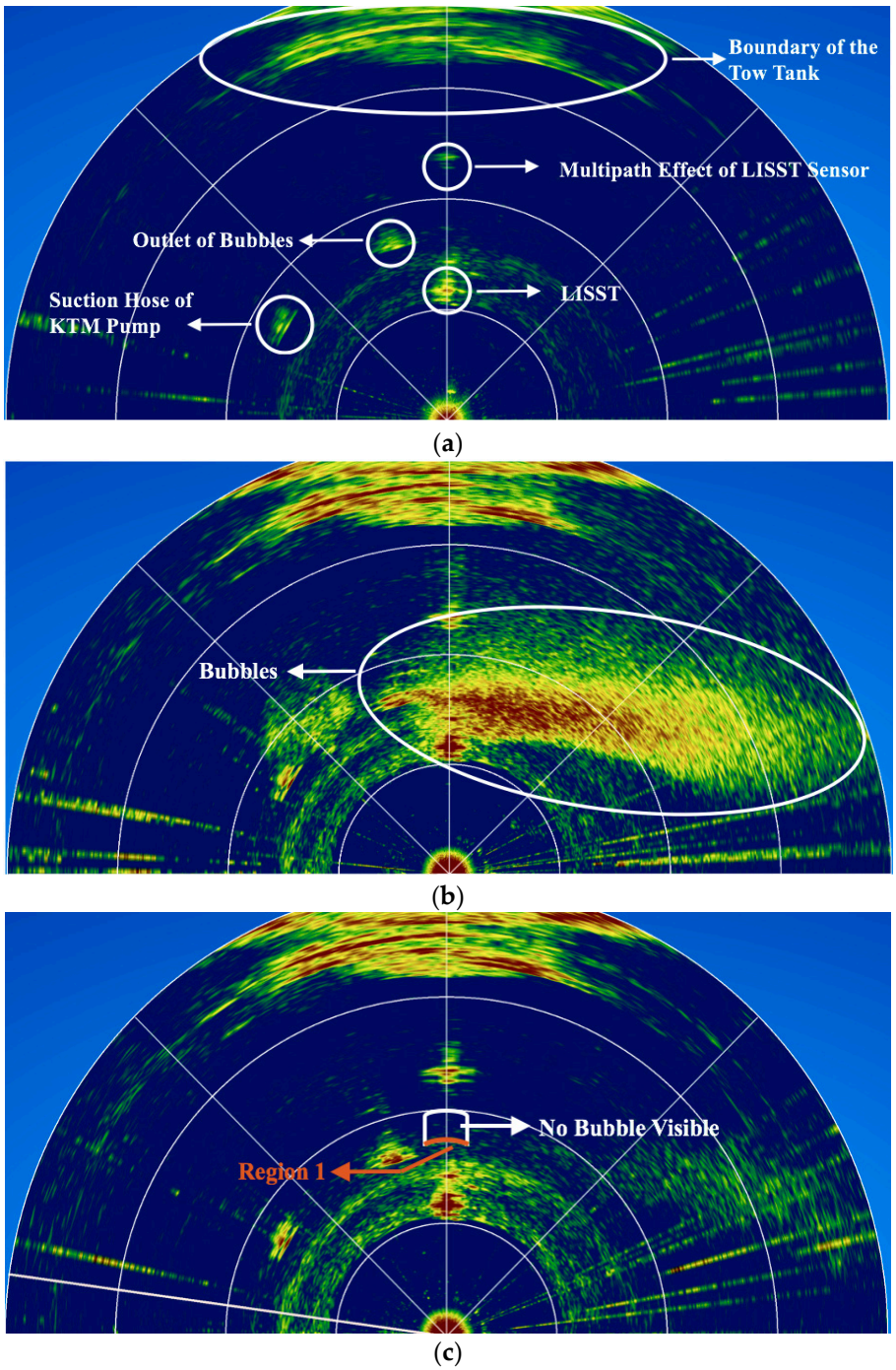

Figure 14. Sonar image collecting at sampling position 3 (**a**) before the start of the bubble generator (**b**) with the bubble generator working (**c**) and a when there was no plume on the vertical plane for calculating residence time.

5. Discussion

In the experiment, a LISST-200X was used to evaluate the size that a microbubble generator can generate, and a sonar was used to investigate the residence times of bubble plumes generated by the pump in the water column. By comparing the data from the LISST-200X and Ping360 sonar, at the water depth of 1.5 m, a larger proportion of smaller bubbles was observed at a longer distance from the release nozzle; the residence time was also longer. As smaller bubbles have low rise velocities, they took a longer time to surface. This observation cross validates the data collected from the LISST-200X sensor and the sonar. When the depth was reduced to 1 m, the residence time of bubbles was longer away from the release nozzle, and longer than the residence time at the corresponding position at the depth of 1.5 m. Although the size of bubbles collected at the point closest to the release nozzle at the depth of 1.0 m did show a higher percentage of smaller bubbles than at a further distance, the small bubbles that rose up from the depth of 1.5 m could have contributed to the longer residence time at the points further away from the nozzle. At the water depth of 0.5 m, a larger proportion of bubbles smaller than 200 microns was collected at a distance of 0.5, closest to the nozzle; however, the residence time at this location was shorter than the other two positions. This could be due to different bubble concentrations at different positions within the plume. For the depth of 0.5 m, a higher concentration of bubbles was found at the distance of 1 m where the longest residence time was observed.

From the sonar images of the experiment conducted in the tow tank, the generated bubble plumes were invisible at approximately 6 m from the release nozzle. In this experiment, there were no waves or current and thus the influence of waves and currents on the motion of the bubble plumes was not tested. When releasing microbubbles in the ocean, waves and currents may have various effects on the plume; they may help extend the outer boundary of the plume providing the AUVs with larger survey area but may also cause the bubble clouds to disperse so thinly that they are undetectable by sonars.

Our next step will be to test this KTM pump and the sonar in the ocean before being applied in AUV missions. It is expected that the bubbles will stay for a longer time than the residence time observed in the lab experiment by releasing the bubbles from deeper water. Moreover, it is also expected that the disturbance from waves and current could drive the bubbles to a further distance from the release nozzle and break the plume into patches of bubble clouds in the water.

6. Conclusions

In this work, an experiment was conducted in a lab to investigate the possibility of using gas bubbles as proxies for oil in AUV field missions. The main interest of this investigation was the residence time and distribution of gas bubble plumes in the water column. The residence time and distribution of gas bubble plumes can represent the buoyant characteristics of gas bubbles and the length of time of bubbles remain in the water column before being detected by acoustic sensors on an AUV. Results from the experiment showed that:

1. A Nikuni KTM pump was able to generate bubbles with sizes less than 100 microns.
2. A Ping360 sonar with a frequency of 750 kHz was found to have the ability to detect microbubble plumes which contain bubbles with sizes less than 100 microns.
3. Smaller bubbles were found at a higher percentage of the total numbers of bubbles in deeper water, such as at the depth of 1.5 m, as large bubbles having higher rise velocities surfaced quickly without staying in the water column.
4. The residence time of the bubble plumes at the depth of 0.5 m was estimated to be over 5 min. The bubbles were generated by the Nikuni KTM pump and released in less than 2 m of water at a depth of 1 m and an inclination angle of 20°.

From the experiment results, it is expected that the residence time of the bubbles can be longer if the bubbles are released from deeper water. The bubble generator developed based on the KTM pump is planned to be applied in future field experiments, as it was effective in producing long-endurance plumes that can be used as a potential proxy for

oil plumes in field trials of AUVs for delineating oil spills. It is also expected that the disturbance from waves and current could drive the bubbles to a further distance from the release nozzle and break the plume into patches of bubble clouds in the water.

Author Contributions: Conceptualization, N.B., W.T., J.H. and Y.W.; methodology, W.T., Y.W. and J.H.; software, Y.W.; validation, Y.W., W.T., C.B. and J.H.; formal analysis, Y.W. and W.T.; investigation, Y.W., W.T., C.B. and J.H.; resources, N.B., Y.W., W.T., J.H. and C.B.; writing—original draft preparation, Y.W., W.T., J.H. and N.B.; writing—review and editing, Y.W., W.T. and J.H., N.B. and C.B.; visualization, Y.W., W.T. and J.H.; supervision, N.B. and W.T.; project administration, N.B.; funding acquisition, N.B. All authors have read and agreed to the published version of the manuscript.

Funding: Funding was received from Fisheries and Oceans Canada through the Multi-Partner Oil Spill Research Initiative (MPRI) 1.03: Oil Spill Reconnaissance and Delineation through Robotic Autonomous Underwater Vehicle Technology in Open and Iced Waters.

Institutional Review Board Statement: Not applicable.

Informed Consent Statement: Not applicable.

Data Availability Statement: Not applicable.

Conflicts of Interest: The authors declare no conflict of interest. The funders had no role in the design of the study; in the collection, analyses, or interpretation of data; in the writing of the manuscript, or in the decision to publish the results.

References

1. Saadoun, I.M.K. Impact of Oil Spills on Marine Life. In *Emerging Pollutants in the Environment-Current and Further Implications*; InTech: Lonon, UK, 2015; pp. 75–104.
2. Socolofsky, S.A.; Adams, E.E.; Sherwood, C.R. Formation dynamics of subsurface hydrocarbon intrusions following the Deepwater Horizon blowout. *Geophys. Res. Lett.* **2011**, *38*, 1–6. [CrossRef]
3. North, E.W.; Adams, E.E.; Thessen, A.E.; Schlag, Z.; He, R.; Socolofsky, S.A.; Masutani, S.M.; Peckham, S.D. The influence of droplet size and biodegradation on the transport of subsurface oil droplets during the Deepwater Horizon spill: A model sensitivity study. *Environ. Res. Lett.* **2015**, *10*, 1–12. [CrossRef]
4. Chan, G.K.Y.; Chow, A.C.; Adams, E.E. Effects of droplet size on intrusion of sub-surface oil spills. *Environ. Fluid Mech.* **2015**, *15*, 959–973. [CrossRef]
5. Conmy, R.N.; Coble, P.G.; Farr, J.; Wood, A.M.; Lee, K.; Pegau, W.S.; Walsh, I.D.; Koch, C.R.; Abercrombie, M.I.; Miles, M.S.; et al. Submersible optical sensors exposed to chemically dispersed crude oil: Wave tank simulations for improved oil spill monitoring. *Environ. Sci. Technol.* **2014**, *48*, 1803–1810. [CrossRef] [PubMed]
6. Pang, S.; Farrell, J.A. Chemical plume source localization. *IEEE Trans. Syst. Man Cybern. Part B Cybern.* **2006**, *36*, 1068–1080. [CrossRef]
7. Hwang, J.; Bose, N.; Fan, S.; Robinson, B.; Tenekedjiev, K. Complications of robotic delineation of oil spills at sea. In Proceedings of the 20th Commemorative Annual General Assembly, AGA 2019-Proceedings of the International Association of Maritime Universities Conference, IAMUC 2019, Tokyo, Japan, 30 October–1 November 2019; pp. 26–33.
8. Hwang, J.; Bose, N.; Robinson, B.; Nguyen, H. Assessing hydrocarbon presence in the waters of port au port bay, newfoundland and labrador, for auv oil spill delineation tests. *J. Ocean Technol.* **2020**, *15*, 100–112.
9. Eriksen, P.K. Leakage and oil spill detection utilizing active acoustic systems. In Proceedings of the 2013 IEEE International Underwater Technology Symposium, Tokyo, Japan, 5–8 March 2013; pp. 1–8.
10. López-Castejón, F.; Gilabert, J. (Eds.) *Underwater Robotics ready for Oil Spill*; Technical Paper URready4OS Project; URready4OS: Cartagena, Spain, 2019; Volume 2, pp. 1–98.
11. Battelle. *Capabilities and Uses of Sensor-Equipped Ocean Vehicles for Subsea and Surface Detection and Tracking of Oil Spills*; Battelle: Columbus, OH, USA, 2014.
12. Pärt, S.; Kõuts, T. *In-Situ Oil Detection Sensor–Technology Overview and Experiment Design WP1: Oil Spill Detection, Monitoring, Fate and Distribution*; Tallinn University of Technology: Tallinn, Estonia, 2016.
13. Tsuge, H. *Micro- and Nanobubbles: Fundamentals and Applications*; Tsuge, H., Ed.; Jenny Stanford Publishing: Singapore, 2014; ISBN 9789814463119.
14. Tamura, I.; Adachi, K. Developing a micro-bubble generator and practical system for purifying contaminated water. *Stud. Sci. Technol.* **2014**, *3*, 87–90. [CrossRef]
15. Khuntia, S.; Majumder, S.K.; Ghosh, P. Microbubble-aided water and wastewater purification: A review. *Rev. Chem. Eng.* **2012**, *28*, 191–221. [CrossRef]

16. Panetta, P.D.; Bland, L.G.; Cartwright, G.; Friedrichs, C.T. Acoustic scattering to measure dispersed oil droplet size and sediment particle size. In Proceedings of the OCEANS 2012 MTS/IEEE: Harnessing the Power of the Ocean, Hampton Roads, VA, USA, 14–19 October 2012; pp. 1–9.
17. Maksym, T.; Singh, H.; Bassett, C.; Lavery, A.; Freitag, L.; Sonnichsen, F. *Oil Spill Detection and Mapping under Arctic Sea Ice Using Autonomous Underwater Vehicles*; Bureau of Safety and Environmental Enforcement: New Orleans, LA, USA, 2014.
18. Wen, R.; Sinding-Larsen, R. Mapping oil seeps on the sea floor by gloria side-scan sonar images-A case study from the Northern Gulf of Mexico. *Nat. Resour. Res.* **1996**, *5*, 141–154. [CrossRef]
19. Wendelboe, G.; Fonseca, L.; Eriksen, M.; Hvidbak, F.; Mutschler, M. Detection of heavy oil on the seabed by application of a 400 kHz multibeam echo sounder. In Proceedings of the 32nd AMOP Technical Seminar on Environmental Contamination and Response, Ottawa, ON, Canada, 9–11 June 2009; Volume 2, pp. 791–816.
20. Parthiot, F.; de Nanteuil, E.; Merlin, F.; Zerr, B.; Guedes, Y.; Lurton, X.; Augustin, J.-M.; Cervenka, P.; Marchal, J.; Sessarego, J.P.; et al. Sonar detection and monitoring of sunken heavy fuel oil on the seafloor. In Proceedings of the Interspill, Trondheim, Norway, 14–17 June 2004; pp. 1–13.
21. Bello, J.; Eriksen, P.; Pocwiardowski, P. Oil Leak Detections with a Combined Telescopic Fluorescence Sensor and a Wide Band MultiBeam Sonar. *Int. Oil Spill Conf. Proc.* **2017**, *2017*, 1559–1573. [CrossRef]
22. Clarke, J.E.H. *Gas Plumes Analysis Using Multibeam EM710 Water Column Image in Saint John River Hesham Elhegazy*; University of New Brunswick: Brunswick, NB, Canada, 2011.
23. Camilli, R.; Di Iorio, D.; Bowen, A.; Reddy, C.M.; Techet, A.H.; Yoerger, D.R.; Whitcomb, L.L.; Seewald, J.S.; Sylva, S.P.; Fenwick, J. Acoustic measurement of the Deepwater Horizon Macondo well flow rate. *Proc. Natl. Acad. Sci. USA* **2012**, *109*, 20235–20239. [CrossRef] [PubMed]
24. Fitzpatrick, M.; Balsley, A.; Hansen, K.A. *Detection of Oil in Water Column, Final Report: Detection Prototype Tests*; U.S. Department of Homeland Security: Washington, DC, USA, 2014.
25. Baszanowska, E.; Otremba, Z. Fluorometry in application to fingerprint of petroleum products present in the natural waters. *J. Eur. Opt. Soc.* **2016**, *12*, 1–9. [CrossRef]
26. Bello, J.M.; Eriksen, P.; Pocwiardowski, P. *Report to BSEE: Oil Leak Detections with a Combined Fluorescence Polarization Instrument and a Wide Band MultiBeam Sonar Phase II Final Report Work Performed Under Contract E14PC00033 Bureau of Safety and Environmental Enforcement (BSEE) Oil Spill Response Research Branch*; Bureau of Safety and Environmental Enforcement: New Orleans, LA, USA, 2016.
27. Wilkinson, J.; Maksym, T.; Singh, H. *Capabilities for Detection of Oil Spills under Sea Ice from Autonomous Underwater Vehicles*; The International Association of Oil & Gas Producers (IOGP): London, UK, 2013.
28. Loranger, S.C. *Acoustic Detection and Quantification of Crude Oil*; University of New Hampshire: Durham, NH, USA, 2019.
29. Fitzpatrick, M.; Tebeau, P.A. *Detection of Oil in Water Column: Sensor Design*; U.S. Department of Homeland Security: Washington, DC, USA, 2013.
30. Scandella, B.; Urban, P.; Delwiche, K.; Greinert, J.; Hemond, H.; Ruppel, C.D.; Juanes, R.; Scandella, B.; Urban, P.; Delwiche, K.; et al. Quantifying methane flux from lake sediments using multibeam sonar. In Proceedings of the American Geophysical Union Fall Meeting, San Francisco, CA, USA, 9–13 December 2013. Abstract id: B53B-0456.
31. Veloso, M.; Greinert, J.; Mienert, J.; De Batist, M. A new methodology for quantifying bubble flow rates in deep water using splitbeam echosounders: Examples from the Arctic offshore NW-Svalbard. *Limnol. Oceanogr. Methods* **2015**, *13*, 267–287. [CrossRef]
32. Leifer, I.; Chernykh, D.; Shakhova, N.; Semiletov, I. Sonar gas flux estimation by bubble insonification: Application to methane bubble flux from seep areas in the outer Laptev Sea. *Cryosphere* **2017**, *11*, 1333–1350. [CrossRef]
33. Uchimoto, K.; Nishimura, M.; Xue, Z.; Watanabe, Y. A preliminary experiment on the detection of bubbles in the sea with side-scan sonar. In Proceedings of the 14th Greenhouse Gas Control Technologies Conference, 14th Greenhouse Gas Control Technologies Conference, Melbourne, Australia, 21–26 October 2018; pp. 1–9.
34. Von Deimling, J.S.; Greinert, J.; Chapman, N.R.; Rabbel, W.; Linke, P. Acoustic imaging of natural gas seepage in the North Sea: Sensing bubbles controlled by variable currents. *Limnol. Oceanogr. Methods* **2010**, *8*, 155–171. [CrossRef]
35. Klaucke, I.; Sahling, H.; Bürk, D.; Weinrebe, W.; Bohrmann, G. Mapping deep-water gas emissions with sidescan sonar. *Eos Trans. Am. Geophys. Union* **2005**, *86*, 341–346. [CrossRef]
36. Crone, T.J.; Tolstoy, M. Magnitude of the 2010 Gulf of Mexico oil leak. *Science* **2010**, *330*, 634. [CrossRef]
37. Weber, T.C.; De Robertis, A.; Greenaway, S.F.; Smith, S.; Mayer, L.; Rice, G. Estimating oil concentration and flow rate with calibrated vessel-mounted acoustic echo sounders. *Proc. Natl. Acad. Sci. USA* **2012**, *109*, 20240–20245. [CrossRef]
38. David, L.; Mudge, T. *Acoustic Detection of Subsurface Oil*; ASL Environmental Sciences: Victoria, BC, Canada, 2018.
39. Szczucka, J. Acoustic Detection of Gas Bubbles in the Sea. *Oceanologia* **1989**, *28*, 103–113.
40. Johansen, Ø.; Rye, H.; Cooper, C. DeepSpill-Field study of a simulated oil and gas blowout in deep water. *Spill Sci. Technol. Bull.* **2003**, *8*, 433–443. [CrossRef]
41. Balsley, A.; Hansen, K.; Fitzpatrick, M. Detection of oil within the water column. In Proceedings of the International Oil Spill Conference, Savannah, GA, USA, 5–8 May 2014; pp. 2206–2217.
42. Blomberg, A.E.A.; Sæbø, T.O.; Hansen, R.E.; Pedersen, R.B.; Austeng, A. Automatic Detection of Marine Gas Seeps Using an Interferometric Sidescan Sonar. *IEEE J. Ocean. Eng.* **2017**, *42*, 590–602. [CrossRef]

43. Hwang, J.; Bose, N.; Nguyen, H.D.; Williams, G. Acoustic search and detection of oil plumes using an autonomous underwater vehicle. *J. Mar. Sci. Eng.* **2020**, *8*, 618. [CrossRef]
44. Zedel, L.; Butt, S. Using micro-bubbles as acoustic targets for large scale fluid flow experiments. In Proceedings of the 2011 IEEE/OES/CWTM 10th Working Conference on Current, Waves and Turbulence Measurement, CWTM, Monterey, CA, USA, 20–23 March 2011; pp. 224–229.
45. Etchepare, R.; Oliveira, H.; Nicknig, M.; Azevedo, A.; Rubio, J. Nanobubbles: Generation using a multiphase pump, properties and features in flotation. *Miner. Eng.* **2017**, *112*, 19–26. [CrossRef]
46. Aeration & Mixing Ltd. Nikuni KTM Gas-Mixing Fine Bubble Generating Pumps. Available online: https://www.aerationmixing.co.uk/products/nikuni-ktm-gas-mixing-fine-bubble-generating-aerator-pumps/ (accessed on 27 October 2020).
47. BlueROV2-Affordable and Capable Underwater ROV. Available online: https://bluerobotics.com/store/rov/bluerov2/ (accessed on 1 March 2020).
48. Sequoia Scientific. *LISST-200X Particle Size Analyzer User's Manual*; Sequoia Scientific, Inc.: Bellevue, WA, USA, 2020.
49. BlueRobotics Ping360 Scanning Imaging Sonar for ROVs. Available online: https://bluerobotics.com/store/sensors-sonars-cameras/sonar/ping360-sonar-r1-rp/ (accessed on 27 October 2020).